World Conference on
Timber Engineering
Oslo 2023

NUMERICAL MODELLING OF MASS TIMBER BEAM-COLUMN CONNECTIONS

Labuwatte Manathum Milindu B Jayasekara[1], Robert M Foster[2]

ABSTRACT: Multi-storey timber buildings are becoming increasingly popular due to advancements in engineered timber technology. Sophisticated timber connections in such buildings play a critical role in both the performance and safety of the structure, particularly in accidental and earthquake situations. Therefore, a thorough understanding of timber connection behaviour is necessary for safe and efficient building design. However, few existing studies capture timber connection behaviours in a sufficiently comprehensive manner to be applied to the complex loading conditions that can occur in accidental situations. This study develops a computational modelling approach that can predict intricate pre- and post-failure behaviours of timber beam-column connections under various loading conditions. First, the commercially available Finite Element software package Abaqus was used to model a timber beam-column connection. Then, nonlinear quasi-static analyses were performed under shear and moment conditions. Finally, sensitivity analyses were conducted to ensure that the model produces consistent results. The computational results obtained agree well with experimental results available in the literature. The developed numerical modelling approach is thus shown to have potential for simulating the complicated behaviour of timber connections under loads and, hence, for the design of safe, efficient timber connections.

KEYWORDS: Disproportionate collapse, Computational mechanics, Damage modelling, Timber connections, LVL

1 INTRODUCTION

Engineered timber is built up from mechanically or adhesively connected timber lamellae to form larger, more homogeneous structural sections suitable for the construction of larger timber structures. Engineered timber is increasingly seen as an alternative to conventional construction materials such as concrete and steel for reducing CO_2 emissions in the construction sector [1] - [2]. As a result, engineered timber is now being used extensively in multi-storey building construction [3].

Commonly used engineered timber products are glued laminated timber (glulam), laminated veneer lumber (LVL) and cross-laminated timber (CLT) [4]. These materials are predominantly used in three main building types [5]: Light-timber frame structures, composed of dimensional lumber and engineered timber that are regularly spaced and fastened together to create floor and wall cassettes: CLT buildings, composed of solid CLT floor and wall panels in a platform-type construction arrangement: and post-and-beam structures, consisting of continuous vertical posts and horizontal beams that are, usually, pin-connected to each other. Post-and-beam structures are thought to offer the greatest potential for realising timber buildings taller than 10 storeys [6] and the heights of such buildings are rapidly increasing [7].

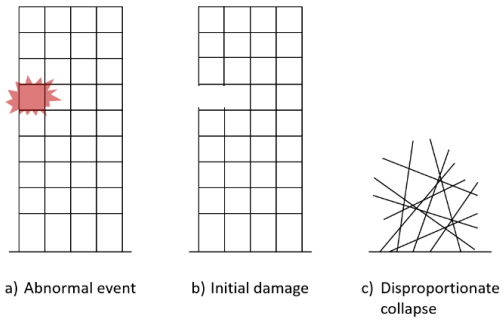

Figure 1: *Disproportionate collapse*

The greater the heights of timber buildings, the more acute the need for thoughtful consideration of abnormal conditions such as fire [8] or disproportionate collapse in design. Disproportionate collapse is a structural collapse in which there is a pronounced disproportion between the initial damage caused by an abnormal event and the extent of the ensuing collapse [9]. A graphical representation of

[1] Labuwatte Manathum Milindu B Jayasekara, PhD Student, Department of Engineering, University of Cambridge, United Kingdom, lmmbj2@cam.ac.uk
[2] Robert M Foster, University Assistant Professor, Department of Engineering, University of Cambridge, United Kingdom, rmf41@cam.ac.uk

https://doi.org/10.52202/069179-0372

this concept is depicted in Figure 1. The key design strategy against this phenomenon is to ensure adequate resistance against failure propagation, i.e., robustness. By limiting the initial damage progression from (b) to (c) in Figure 1, a sufficiently robust structure can be obtained.

Timber beam-column connections, which are often made of steel or aluminium, play a vital role in ensuring reliable robustness of multi-storey timber buildings. These connections provide ductility and continuity to buildings, and with sufficient strength and deformation capacities, they can allow the formation of alternative load paths (ALPs) during initial damage [10] - [11]. These ALPs bridge or bypass a local failure zone; preventing failure propagation throughout the structure and hence averting disproportionate collapse. Examples of such ALPs are catenary, arching and membrane actions [12]. Understanding connection performance under load is thus crucial for achieving a robust building design. However, limited literature is available on timber post-beam connection behaviour [13] - [14].

Computational methods can be a cost-effective and efficient approach for capturing connection behaviours. With recent developments in computational mechanics and failure theories, it may be possible to simulate isotropic metals, anisotropic timber and their combined behaviour in timber connections beyond initial failure. The majority of existing studies are limited to linear elastic-plastic behaviour [15] or simple dowel-type connections [16] or one material/parameter performance [17]. Some studies employ pre-defined failure surfaces to initiate failure [18] - [19] but these may not be suitable for all types of loading because of the need to predefine failure. In addition, the numerical solving methods used in these studies may not be suitable to simulate complex pre- and post-failure material behaviour in timber connections [20]. Therefore, a comprehensive modelling technique is required to capture the behaviours of timber connections under any mechanical loading condition.

This research project aims to develop a computational modelling technique that can capture complex pre- and post-failure behaviour of timber beam-column connections under various loads. This paper presents the initial stages of building the complete computational model. First, material properties and connector details are outlined. Second, the modelling approach and results are discussed. Third, a parametric study is demonstrated. Finally, the conclusions of the study so far are presented.

2 TIMBER CONNECTION

A T-section connector tested by Masaeli et al. [21] and shown in Figure 2 was selected from the literature as an initial experimental benchmark for the development of the computational modelling technique. Full experimental details are provided by Masaeli et al [21] with key properties reproduced here. The tests used Douglas fir LVL timber column and beam sections of sizes 360 × 360 mm^2 and 600 × 252 mm^2 respectively. The T-section was made of AW 6005-A aluminium alloy, and the connection was composed of two rows of six 16 mm (M16 grade 8.8) bolts and ten 16 mm steel dowels (S355). The connector was tested experimentally under shear and moment quasi-statically [21], and the testing arrangements adopted are illustrated in Figure 3. These experimental results are used in this paper to evaluate the performance of the Finite Element (FE) model.

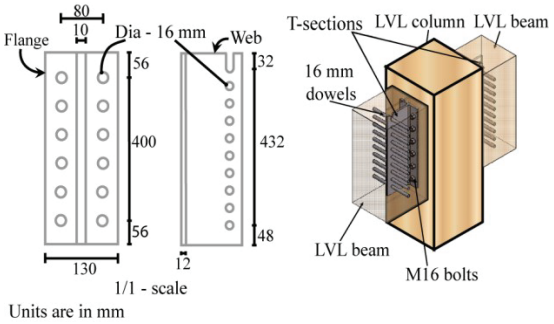

Figure 2: *T-connector details, redrawn after Masaeli et al. [21]*

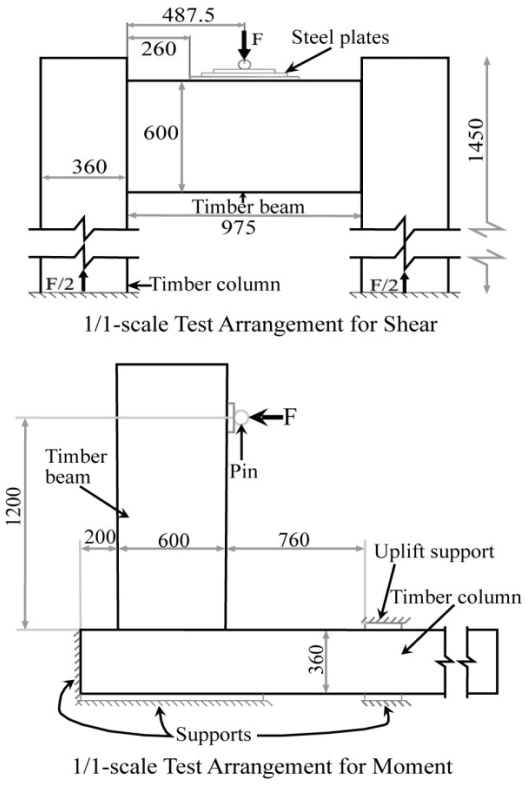

Figure 3: *Experimental testing setups, redrawn after Masaeli et al. [21]*

Material properties adopted in the FE analyses are given in Table 1 and Table 2 for timber and metals respectively.

The majority of these material properties including Young's modulus (E), Poisson's ratio (υ), shear modulus (G) and shear strengths (f_v) are those reported by Masaeli et al. [21]. Strains (ε) for metals are obtained from the wider literature [22]. Steel and aluminium are considered as isotropic materials whereas timber is modelled as an orthotropic material. Principal material directions for timber are depicted in Figure 4.

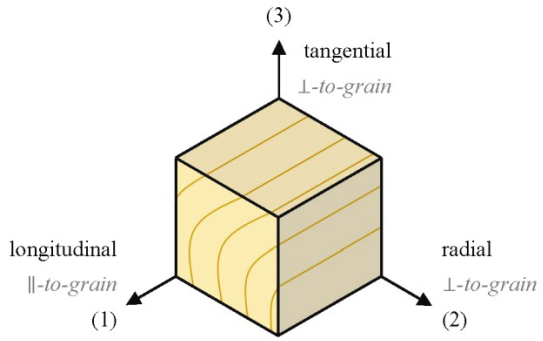

Figure 4: *Timber material directions*

Numerical subscripts for each timber material property represent these principal directions. Subscripts "c", "v", "y" and "m" denote compression, shear, yield and maximum respectively. "f", "σ", "ε_m" and "ε_{tf}" refer to strength, stress, engineering strain at maximum stress and true fracture strain respectively.

Table 1: *Material properties for LVL timber [21]*

Parameter	Unit	Value
E_{11}	MPa	15500
$E_{22} = E_{33}$	MPa	470
$\upsilon_{12} = \upsilon_{13}$		0.37
υ_{23}		0.38
$G_{12} = G_{13}$	MPa	660
G_{23}	MPa	132
f_{c11}	MPa	46.4
$f_{c22} = f_{c33}$	MPa	8.8
$f_{v12} = f_{v13}$	MPa	7
f_{v23}	MPa	1.4

Table 2: *Material properties of metals [21] - [22]*

Parameter	Unit	Bolt	Dowel	Connector
Density	kg/m^3	8050	8050	2710
E	GPa	207	209	70
υ		0.3	0.3	0.23
σ_y	MPa	861	556	187
σ_m	MPa	956	597	221
ε_m		0.09	0.1	0.0553
ε_{tf}		1.03	0.90	1.10

3 FINITE ELEMENT MODEL

All the parts of the connection were drawn separately and assembled as depicted in Figure 5 using the FE software package Abaqus [23].

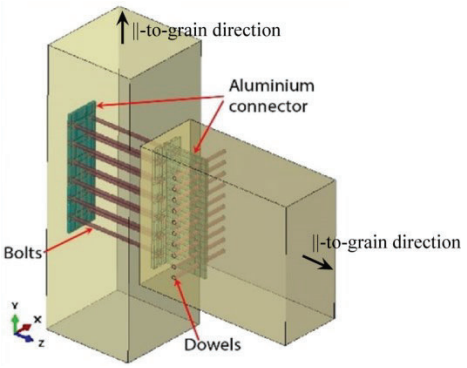

Figure 5: *FE model of the timber beam-column connection*

For the aluminium connector, small 8 mm chamfers were introduced at 90^0-degree corners to avoid numerical singularities. To define relationships between the components, 35 separate contact interactions were defined and constitutive models for metals and timber were specified to simulate their individual behaviour under loads. After performing a mesh sensitivity analysis for each component, boundary conditions and loadings were applied to simulate both shear and moment behaviour of the connector. These are discussed in detail in this section.

3.1 HILL CRITERION FOR TIMBER

The constitutive relationship for timber is defined in this study assuming orthotropic material properties. Only the ductile behaviour of timber under compression was considered in this paper. An elastic-perfectly plastic material model based on the Hill criterion with anisotropic yielding was employed using the properties given in Table 1. The Hill criterion has been successfully used in timber modelling to define plastic yielding [24]. Equation (1) shows the Hill criterion. Yielding occurs when the function reaches the value of 1.

$$f(\sigma) = [F(\sigma_{22} - \sigma_{33})^2 + G(\sigma_{33} - \sigma_{11})^2 + H(\sigma_{11} - \sigma_{22})^2 + 2L\sigma_{23}^2 + 2M\sigma_{31}^2 + 2N\sigma_{12}^2] \quad (1)$$

where:

$$F = \frac{1}{2}\left(\frac{1}{R_{22}^2} + \frac{1}{R_{33}^2} - \frac{1}{R_{11}^2}\right)$$

$$G = \frac{1}{2}\left(\frac{1}{R_{33}^2} + \frac{1}{R_{11}^2} - \frac{1}{R_{22}^2}\right)$$

$$H = \frac{1}{2}\left(\frac{1}{R_{11}^2} + \frac{1}{R_{22}^2} - \frac{1}{R_{33}^2}\right)$$

$$L = \left(\frac{3}{2R_{23}^2}\right), M = \left(\frac{3}{2R_{13}^2}\right), N = \left(\frac{3}{2R_{12}^2}\right)$$

$$R_{11}^2 = \frac{f_{c11}}{f^0}, R_{22}^2 = \frac{f_{c22}}{f^0}, R_{33}^2 = \frac{f_{c33}}{f^0}$$

$$R_{12}^2 = \frac{f_{v12}}{\tau^0}, R_{13}^2 = \frac{f_{v13}}{\tau^0}, R_{23}^2 = \frac{f_{v23}}{\tau^0}$$

https://doi.org/10.52202/069179-0372

where f^0 is the reference yield stress and $\tau^0 = f^0/\sqrt{3}$.

3.2 PLASTICITY MODEL FOR DUCTILE MATERIALS

An elastic-plastic material model was applied for ductile metals. Material properties given in Table 2 were utilised to obtain the engineering stress-strain curves for bolts, dowels and aluminium connector. Yielding was defined using the Von Mises yield surface with isotropic hardening. This criterion has shown promising results in the literature [22]. Von Mises yield criterion is given in Equation (2) and yielding occurs when $\sigma_v \geq \sigma_y$:

$$\sigma_v^2 = \frac{1}{2}[(\sigma_{aa} - \sigma_{bb})^2 + G(\sigma_{bb} - \sigma_{cc})^2 + (\sigma_{cc} - \sigma_{bb})^2 + 6(\sigma_{bc}^2 + \sigma_{ca}^2 + \sigma_{ab}^2)] \quad (2)$$

where σ_v is the Von Mises (equivalent) stress and a, b, c are the principal material directions.

Abaqus requires an equivalent stress-strain curve as input to simulate this yielding of metals. Therefore, engineering stress-strain curves were first converted to true stress-strain curves using Equation (3) and Equation (4):

$$\sigma_t = \sigma_e(1 + \varepsilon_e) \quad (3)$$

$$\epsilon_t = ln(1 + \varepsilon_e) \quad (4)$$

where σ_t is the true stress, σ_e is the engineering stress, ϵ_t is the true strain and $\varepsilon_e$is the engineering strain. As these equations are valid only up to necking, Hollomon's extrapolation method [25] was used to obtain the full curve. The true stress-strain curves were then converted to equivalent stress-strain curves, noting that the true stress-strain curve and equivalent stress-strain curve up to necking are the same. After necking, the Gromada correction factor was applied to account for the tri-axial stress state [25]. The resulting equivalent stress-strain curves are presented in Figure 6. Continuum damage modelling techniques were also employed after necking to simulate the ductile failure of materials [23].

3.3 MESH

Separate mesh sensitivity analyses were conducted for each component of the connection. From these, a suitable mesh arrangement was chosen for each component to maintain accuracy. A total of 268502 8-node linear hexahedral elements (C3D8R) are used in this model. Reduced integration and relax-stiffness hourglass options were included in these elements to minimise shear locking, computational effort and zero-energy deformation modes.

3.4 CONTACTS AND BOUNDARY CONDITIONS

The general contact algorithm in Abaqus was utilized with element-based surface definitions to define contacts in the connection model. These element-based contact surface pairs were specified individually to avoid numerical problems and unwanted energies. To simulate the sliding behaviour of these contacts, a friction coefficient of 0.3 was applied for the tangential direction. For the normal direction, a generalised Lame function proposed by Dorn [26] was employed to characterise pressure-overclosure (resistance to penetration) behaviour of surfaces. This accounts for the softening of timber near bolts and dowel holes.

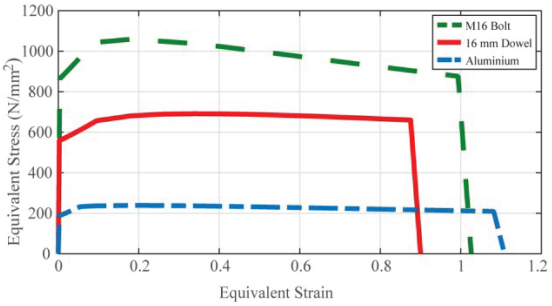

Figure 6: *Equivalent stress-strain curves of bolts, dowels and aluminium connector*

For numerical efficiency, finite sliding with balanced contact weighting was used. This is beneficial for simulating large deformations and for minimising unrealistic node penetrations in contact surfaces. Furthermore, a penalty constraint was also applied to allow these small penetrations in contacts and, therefore, to reduce artificial resisting forces that can cause numerical instabilities. This is particularly useful when circular shapes, such as bolts and dowels, are included in the model.

Boundary conditions were also employed to replicate both shear and moment loading conditions for the connection. The top and bottom surfaces of the column were fixed as shown in Figure 7. A distance of 250 mm between the connector and the fixed boundary conditions was kept to eliminate influence from the fixity to the connector. For the shear analysis, translational degrees of freedom (DOFs) in x- and y-directions at the end of the beam were restrained to resemble the shear behaviour.

3.5 LOADING

For all the numerical analyses conducted, only displacement-based loads were specified to capture moment and shear responses. First, a small displacement of 10 nm was applied to all the parts near contacts for initiating the contacts and eliminating numerical problems. This imposed displacement was then removed while enforcing new vertical displacements to simulate the required responses of the connector.

These vertical displacements were assigned to reference points using a fifth-order polynomial function until failure occurs [23]. The location of the reference point changes depending on the behaviour the numerical model tries to capture: moment or shear. In the case of the moment test, the end of the beam was constrained to a reference point

https://doi.org/10.52202/069179-0372

using coupling constraints with continuum distribution as illustrated in Figure 8. This constrains the DOFs of the nodes in the connecting surface to the DOFs of the reference point. By doing so, imposed displacement to the reference point is distributed in an average sense to the connecting nodes by producing realistic results. A similar procedure was followed for the shear test, but now the connecting surface is at the top of the beam as shown in Figure 8. Accordingly, from the results of numerical models tested in moment and shear, moment-rotation and load-displacement curves were extracted respectively.

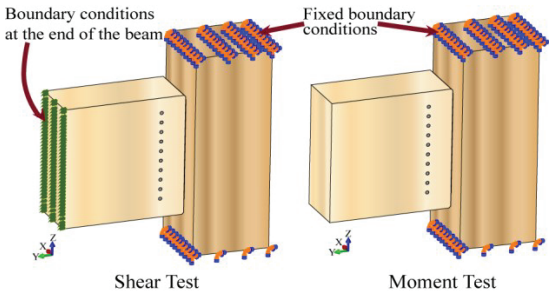

Figure 7: *Boundary conditions of FE models*

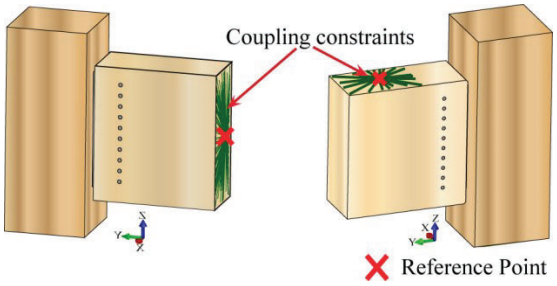

Figure 8: *Coupling constraints and reference points for the moment (left) and shear (right) simulations*

3.6 SOLVER

Owing to the complexities of the behaviour modelled, the commonly used Abaqus standard solver is not suitable for analysing such timber connections. The reason is that this solver solves for equilibrium [23], which means that problems become difficult to solve when a large number of contacts, failure mechanisms and non-linearities are involved. Abaqus explicit solver, on the other hand, solves equations of motion, which means that the calculation remains straightforward, and the overall analysis is efficient. However, this method is more commonly applied for dynamic analyses.

In order to perform a quasi-static analysis using the explicit solver, two sensitivity analyses have to be conducted to keep the kinetic energy acceptably low. One analysis is to identify a load rate that produces zero kinetic energy. It is impractical, even with high-power computing, to recreate the actual load rate used in the experimental tests due to the large number of time increments needed for the analysis. Therefore, a computationally less expensive load rate must be selected. However, increasing the load rate alone may not be sufficient to achieve a computationally efficient analysis.

Mass scaling is another parameter used to aid quasi-static analyses. This speeds up the analysis by increasing the time increment of the solver. However, by doing so, the kinetic energy of the system increases. Therefore, a sensitivity analysis must be performed to find a mass scaling factor. Both these sensitivity analyses are trial-and-error processes. Therefore, a separate dynamic analysis was performed to find the natural frequency of the model, and this was used to decide an initial trial value for the load rate. The resulting selected load rates are 0.25 m s^{-1}, 0.5 m s^{-1} and 1 m s^{-1} and the chosen mass scaling factors are 5, 10 and 20.

The model developed for the moment test was utilised in these two sensitivity analyses. Displacements were applied as described in Section 3.5 using the three different load rates and mass scaling factors. The moment vs rotation plots are shown in Figure 9.

Kinetic energies for each test were also compared to ensure that the kinetic energy is less than 5% of the internal energy. It can be seen that the results converge when the load rate and the mass scaling factor decrease, meaning that kinetic energy is low. Therefore, considering computational cost and kinetic energy, a load rate of 0.25 m s^{-1} and a mass scaling factor of 10 were chosen. The rest of the analyses were conducted using these selected parameters.

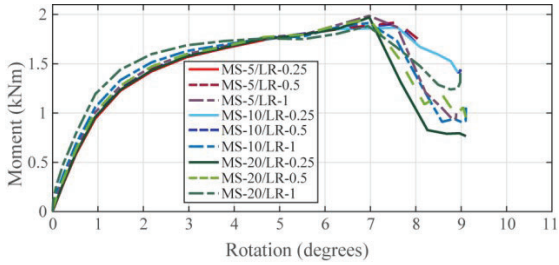

Figure 9: *Sensitivity analysis for mass scaling and load rate*

4 RESULTS AND DISCUSSION

The developed numerical connection model was analysed under shear and moment. Displacement-based loads were applied as described in Section 3.5 with the load rate and mass scaling factor obtained in Section 3.6.

Figure 10 illustrates the moment-rotation prediction in contrast to experimental results in [21]. The computational model captures the moment-rotation response of the connector including post-failure behaviour with good accuracy. The predicted initial stiffness, rotational capacity and maximum moment capacity agree well with the experimental results. It should be noted that, for the maximum moment capacity, there is a deviation of 1% from the average experimental

https://doi.org/10.52202/069179-0372

result. This distinction, however, lies within the experimental envelope and is due to the insignificant dynamic behaviour after elements start to fail. The predicted failure mechanism shown in Figure 11 matches well with the experimental observations of Masaeli et al. [21] – tearing near bolt holes and fracturing at the flange-web interface of the aluminium connector. However, in the FE model, the fracture at the interface is partial in contrast to the experimental fracture.

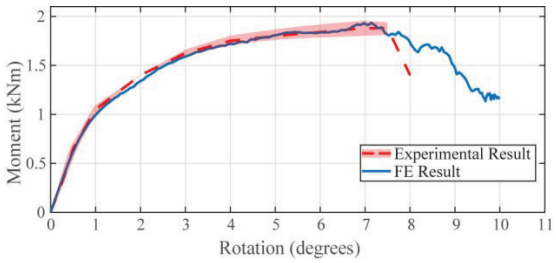

Figure 10: *Experimental [21] and numerical moment vs rotation response*

The shear response of the connector was also estimated and is presented in Figure 12. Overall, the load vs displacement behaviour is similar to the experimental behaviour. However, FE values over-predict the force response and under-predict the displacement response with a maximum variation of 28% and 65% from the average experimental result for the forces and displacements respectively. This may be primarily because of the exclusion of timber brittle failure under tension in these FE models.

As seen in Figure 13, experimentally observed tensile failure perpendicular to grain [21] was not captured in FE simulations. Instead, the applied loads primarily concentrated on the aluminium connector leading to higher resistance and lower displacement capacity. Hence failure occurred in the connector in simulations. Despite this, the numerical model captures the maximum strength capacity well, with a deviation of 2.4%.

In all these analyses, energy outputs of the FE models such as artificial energy, kinetic energy, contact penalty energy, etc., were checked against the recommended limits to ensure that the results are accurate [23].

5 PARAMETRIC STUDY

Parametric studies were conducted to identify the effects of three different parameters. These are discussed in detail in this section.

5.1 BEAM-COLUMN GAP

In the computational models, a small gap between the column and the beam was kept, as displayed in Figure 14. The gap of 23 mm represents the weakened hollow portion of the beam due to machine cut – since this is a concealed connector – and was set to provide 4 mm initial clearance between the bolt nut and the timber. The inclusion of the gap is beneficial in avoiding complicated contacts and reducing computational effort. To explore the influence of this gap, another FE model was developed in which the beam touches the column by fully enclosing the connector. The moment-rotation and load-displacement responses are plotted in Figure 15 and Figure 16 for both models.

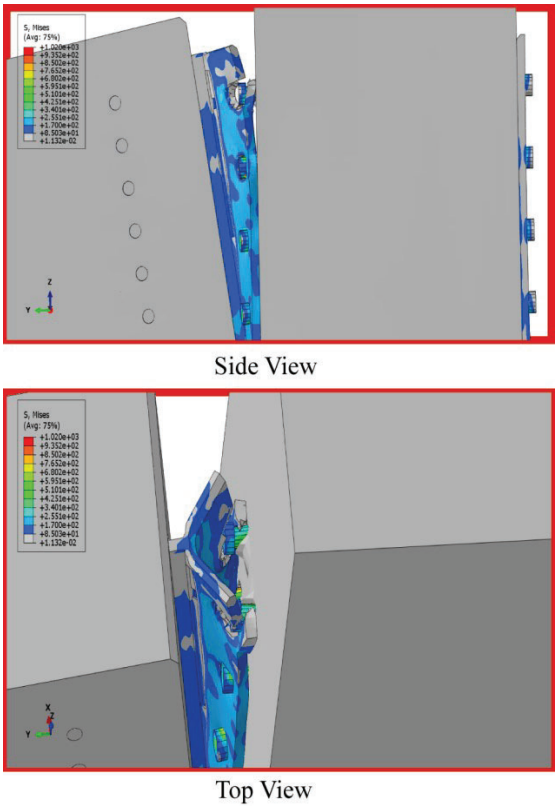

Figure 11: *Failure mode under moment test*

From Figure 15, it can be seen that the results of the FE model without the gap deviate significantly from the experimental results. The maximum moment capacity predicted has a variation of 14.3%. Furthermore, the rotational capacity is under-predicted by approximately 1°. This indicates that if the weakened hollow portion of the beam is not appropriately modelled artificially high resistance against rotation may be observed.

The shear response of the model without the gap shows similar peak resistance but less ductility than the FE model with the gap. For FE models without the gap, a 2.6% higher peak shear resistance and a 30% lower deformation capacity compared to the FE model with the gap were noted, and these may be a result of increased contact area between the connector and the timber beam. Failure modes of both moment and shear simulations are similar to the original FE models. These results suggest that a gap between the column and the beam can be employed to minimise the above-mentioned discrepancies in modelling these types of timber connections.

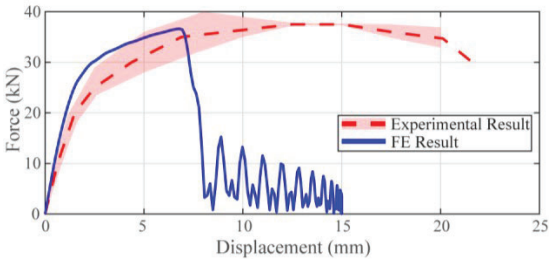

Figure 12: *Experimental [21] and numerical load vs displacement response*

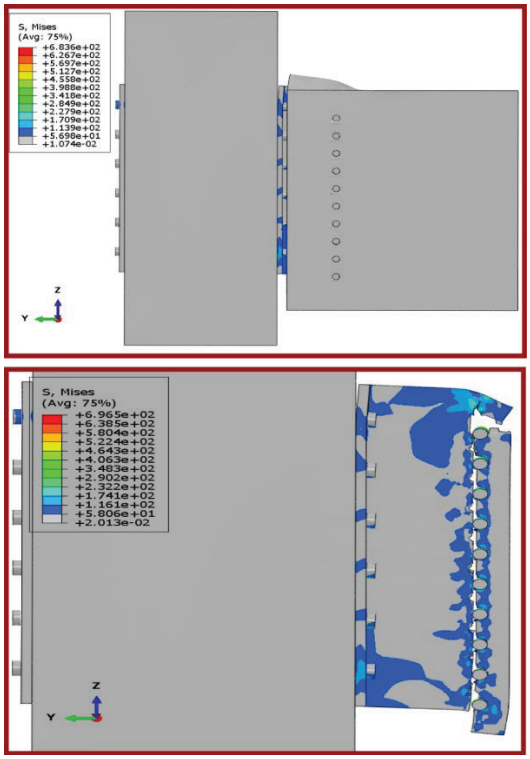

Figure 13: *Failure mode under shear test*

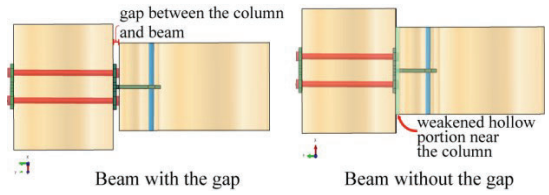

Figure 14: *Column-beam gap*

5.2 CHARACTERISTIC ELEMENT LENGTH

In continuum damage modelling, a total plastic deformation parameter is defined to simulate ductile damage of metals [23]. This parameter is constant for a particular material, and when an element reaches the specified total plastic deformation, element deletion occurs. Total plastic deformation (U^p) is given in Equation (5).

$$U^p = L_c\left(\varepsilon_{tf}^p - \varepsilon_{tn}^p\right) \tag{5}$$

where L_c is the characteristic element length, ε_{tf}^p is the true plastic strain at fracture and ε_{tn}^p is the true plastic strain at necking. ε_{tf}^p and ε_{tn}^p are material properties and are independent of element properties.

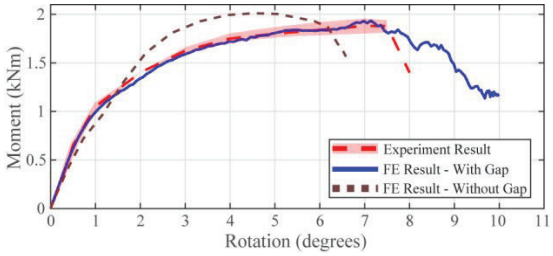

Figure 15: *Experimental [21] and numerical moment vs rotation response of models with and without the gap*

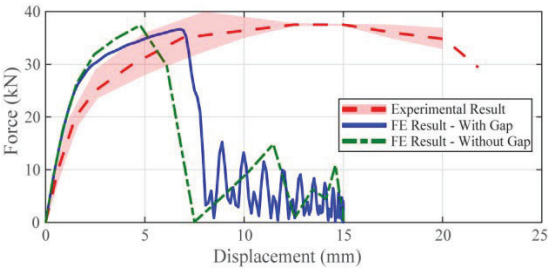

Figure 16: *Experimental [21] and numerical load vs displacement response of models with and without the gap*

Characteristic element length depends on the element geometry and formulation. Same-size elements with an aspect ratio of unity are usually recommended to achieve a uniform L_c in the mesh. If the L_c of elements in the mesh varies significantly from that specified in the damage model, damage behaviour can be different from that defined. As the mesh varies near the holes and the T-joint of the aluminium connector, a sensitivity analysis was conducted for the connector to investigate the impact of L_c on the analysis.

In the original FE model, a value of 2.34 mm was used as L_c for modelling damage in the connector. This value was determined based on the average dimensions of elements in the connector mesh. Another two L_c values were selected for U^p keeping the mesh constant; L_c = 2.10 mm and L_c = 2.60 mm. These two values adequately represent possible element sizes in the mesh. The moment-rotation curves obtained using each L_c value are illustrated in Figure 17.

All three plots follow the same experimental moment-rotation response until approximately 6° of rotation. However, considerable differences between the plots start to appear near the failure point. For L_c = 2.6 mm the analysis over-predicts the maximum moment capacity by 6%, whereas for L_c = 2.1 mm the analysis under-predicts

https://doi.org/10.52202/069179-0372

by 5%. In terms of rotational capacity, L_c = 2.6 mm shows good agreement with the experimental value while L_c = 2.1 mm shows about 1° lower rotational capacity.

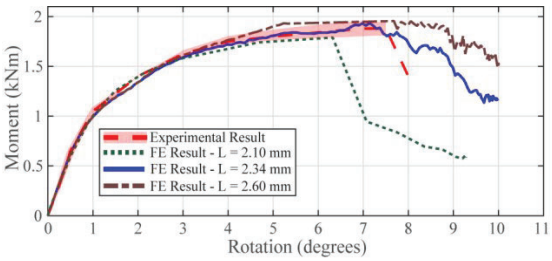

Figure 17: *Experimental [21] and numerical moment vs rotation response for characteristic element length analysis*

Failure modes for L_c = 2.1 mm, L_c = 2.34 mm and L_c = 2.6 mm are shown in Figure 18, Figure 11 and Figure 19 respectively. Three different failure modes were identified. FE models with L_c = 2.1 mm and L_c = 2.34 mm exhibit tearing of aluminium as was seen in experiments, and in the L_c = 2.1 mm model, even the complete fracture near the web-flange interface can be observed. When L_c = 2.6 mm, failure first occurs in the bolts near the column as presented in Figure 19. Failure modes for the shear tests were similar for all three cases as the actual failure occurred in the timber beam.

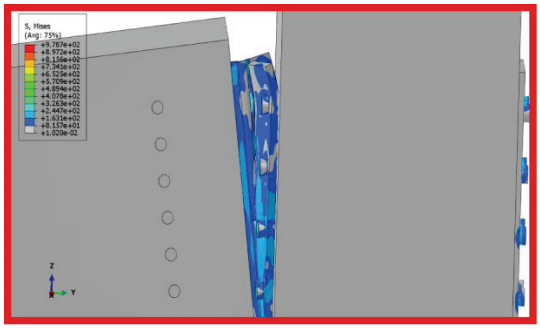

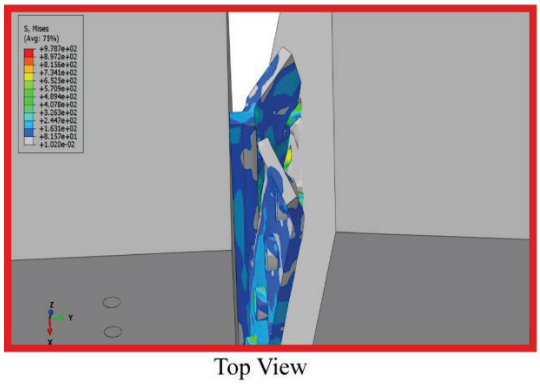

Figure 18: *Numerical failure mode of FE models with L_c = 2.1 mm*

The three failure behaviours observed – tearing and partial fracture, tearing and complete fracture, and bolt failure – are possible alternatives for this connection under moment loading. Therefore, one should consider all such possible mechanisms in order to make predictions and designs if a mesh size of a part varies. In such cases, it is advisable to conduct a parametric study for L_c. This will also take into account the material property variability indirectly in the simulations. Nevertheless, the FE model with average element length may yield overall good results for moment and shear responses.

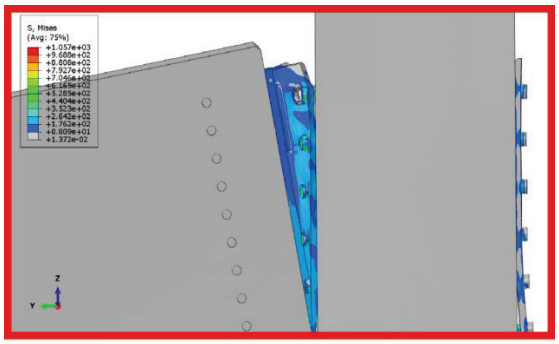

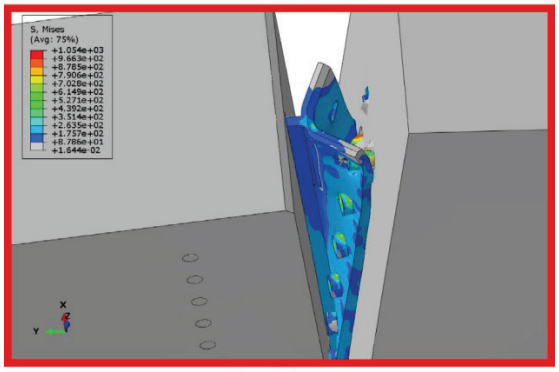

Figure 19: *Numerical failure mode of FE models with L_c = 2.6 mm*

5.3 SYMMETRY OF THE MODEL

To reduce the computational cost, the symmetry of the connection was considered. Based on that, half-models as shown in Figure 20 were created for both moment and shear simulations.

In addition to the boundary conditions and constraints discussed in Section 3.4, symmetric boundary conditions were employed as depicted in Figure 20. Note that, these are applied to the boundary surface excluding the nodes that are involved in contact definitions. This eliminates over-constraint issues. For symmetric boundary conditions, translational DOF in the x-direction and rotational DOFs in the y- and z-directions were restrained. Then, the models were analysed under shear and moment loading conditions to investigate the effectiveness of taking symmetry into account. Moment-rotation and load-displacement curves are shown in Figure 21 and Figure 22, respectively.

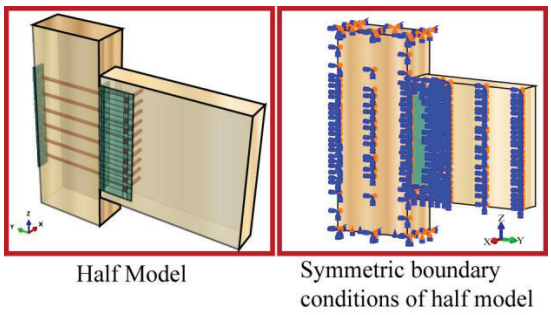

Figure 20: *Half-model and symmetric boundary conditions*

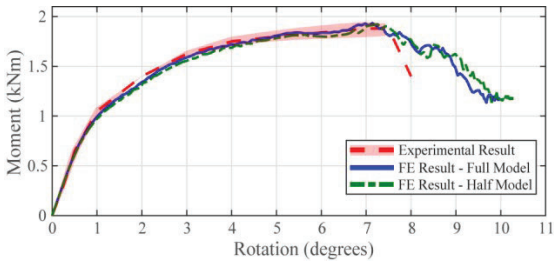

Figure 21: *Experimental [21] and numerical moment vs rotation response of full and half models*

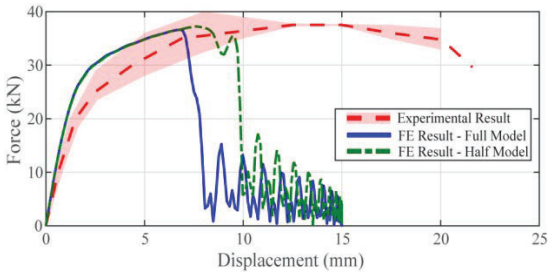

Figure 22: *Experimental [21] and numerical load vs displacement response of full and half models*

The results of the half-model for both moment and shear match closely with the full-model predictions. Therefore, symmetry can be utilised in simulating such timber connections, and this also reduces the computational cost.

6 CONCLUSIONS

This study aims to develop a computational modelling technique that can capture complex pre- and post-failure behaviour of timber beam-column connections under various loads. This paper presents the initial stages of building the complete computational model. A numerical modelling technique was developed using the FE package Abaqus. This technique was then used to analyse a T-section connector under shear and moment to demonstrate the performance of the method. A parametric study was also conducted to increase the accuracy of the model predictions and to evaluate the consistency of the modelling approach adopted. The following conclusions can be drawn:

1. The developed numerical model demonstrates potential in capturing complex pre- and post-failure behaviours of timber connections through large deformations and under different loading situations.
2. For concealed connections, introducing a suitable gap between the column and the beam in the FE models to account for weakening of the hollow portion may provide more realistic results.
3. A sensitivity analysis for the characteristic element length is needed if damage modelling for ductile metals is employed with non-uniform meshes. This is particularly important for FE predictions and designs. An average element length, however, was found to yield overall good results.
4. The symmetry of connections can be taken into account in numerical modelling of connections of this type to improve computational efficiency.

This technique has potential to support design and optimisation of timber connections, especially for robustness. Future works will develop this model to include tensile failure of timber.

ACKNOWLEDGEMENTS

The first author would like to acknowledge Cambridge Commonwealth European and International Trust for the financial support of the Jafar Cambridge Studentship. The authors would also like to thank Prof. Benoit Gilbert and his team at Griffith University, Australia for generously sharing the additional experimental data used in this study.

REFERENCES

[1] R. Sathre, J. O'Connor. Meta-analysis of greenhouse gas displacement factors of wood product substitution. *Environmental Science Policy*, 13(2):104–114, apr 2010.

[2] A. Himes, G. Busby. Wood buildings as a climate solution. *Developments in the Built Environment*, 4:100030, nov 2020.

[3] R. M. Foster, T. P. S. Reynolds. Light weighting with Timber: An Opportunity for More Sustainable Urban Densification. *Journal of Architectural Engineering*, 24(1):02518001, mar 2018.

[4] The Structural Engineer. Engineered wood products and an introduction to timber structural systems. The Institution of Structural Engineers, 2013.

[5] J. A. J. Huber, M. Ekevad, U.A. Girhammar, S. Berg. Structural robustness and timber buildings – a review. *Wood Material Science Engineering*, 14(2):107–128, Mar 2019.

[6] R. Abrahamsen. Mjøstårnet-18 storey timber building completed. In 24. *Internationales Holzbau-Forum IHF*, 2018.

[7] R. M. Foster, M. H. Ramage. Tall Timber. *Nonconventional and Vernacular Construction*

https://doi.org/10.52202/069179-0372

Materials: Characterisation, Properties and Applications [2nd ed.], edited by K. Harries, and B. Sharma, 467–489, 2020. Cambridge: Woodhead Publishing.

[8] A. Law, R. Hadden. We need to talk about timber: fire safety design in tall buildings. *The Structural Engineer*, 3, 2020.

[9] U. Starossek and M. Haberland. Disproportionate Collapse: Terminology and Procedures. *Journal of Performance of Constructed Facilities*, 24(6):519–528, dec 2010.

[10] The Institution of Structural Engineers. Practical guide to structural robustness and disproportionate collapse in buildings. 2010.

[11] P. H. Kirkegaard, J. D. Sørensen, D. Cizmar, and V. Raj˘ci´c. System reliability of timber structures with ductile behaviour. *Engineering Structures*, 33(11):3093–3098, nov 2011.

[12] U. Starossek. Progressive Collapse of Structures. London: Thomas Telford Limited, 2009.

[13] C. H. Lyu, B. P. Gilbert, H. Guan, I. D. Underhill, S. Gunalan, H. Karampour, and M. Masaeli. Experimental collapse response of post-and-beam mass timber frames under a quasi-static column removal scenario. *Engineering Structures*, 213:110562, jun 2020.

[14] C. H. Lyu, B. P. Gilbert, H. Guan, I. D. Underhill, S. Gunalan, and H. Karampour. Experimental study on the quasi-static progressive collapse response of post-and-beam mass timber buildings under an edge column removal scenario. *Engineering Structures*, 228, 111425, 2021.

[15] G. D'Arenzo, G. Rinaldin, M. Fossetti, and M. Fragiacomo. An innovative shear-tension angle bracket for Cross-Laminated Timber structures: Experimental tests and numerical modelling. *Engineering Structures*, 197:109434, oct 2019.

[16] A. Hassanieh, H.R. Valipour, M.A Bradford, C. Sandhaas. Modelling of stee-timber composite connections: validation of finite element model and parametric study. *Engineering Structures*, 138:35-49, Feb 2017.

[17] M. Gharib, A. Hassanieh, H. Valipour, and M. A. Bradford. Three-dimensional constitutive modelling of arbitrarily orientated timber based on continuum damage mechanics. *Finite Elements in Analysis and Design*, 135:79–90, nov 2017.

[18] T. Ge˘cys, A. Daniunas, T.K. Bader, L. Wagner, J. Eberhardsteiner. 3D finite element analysis and experimental investigations of a new type of timber beam-to-beam connection. *Engineering Structures*, 86:134–145, Mar 2015.

[19] X. Cheng, B. P. Gilbert, H. Guan, D. Dias-da-Costa, and H. Karampour. Influence of the earthquake and progressive collapse strain rate on the structural response of timber dowel type connections through finite element modelling. *Journal of Building Engineering*, 57, 104953, 2022.

[20] M. Wang, X. Song, X. Gu, J. Tang. Bolted glulam beam-column connections under different combinations of shear and bending. *Engineering Structures*, 181:281-292, Dec 2018.

[21] M. Masaeli, B. P. Gilbert, H. Karampour, I. D. Underhill, C. H. Lyu, and S. Gunalan. Scaling effect on the moment and shear responses of three types of beam-to-column connectors used in mass timber buildings. *Engineering Structures*, 208:110329, Apr 2020.

[22] E. L. Grimsmo, A. Aalberg, M. Langseth, and A. H. Clausen. Failure modes of bolt and nut assemblies under tensile loading. *Journal of Constructional Steel Research*, 126:15–25, nov 2016.

[23] Dassault Systèmes Simulia Corp. ABAQUS User's Manual, Version 6.14, 2014.

[24] R Hill. A theory of the yielding and plastic flow of anisotropic metals. Proceedings of the Royal Society of London. Series A. *Mathematical and Physical Sciences*, 193(1033):281–297, may 1948.

[25] S. Tu, X. Ren, J. He, Z. Zhang. Stress-strain curves of metalic materials and post-necking stress strain hardening characterization: A review. *Fatigue & Fracture of Engineering Materials and Structures*, 43:3-19, 2020.

[26] M. Dorn, K. Borst, J. Eberhardsteiner. Experiments on dowel-type timber connections. *Engineering Structures*, 47:67–80, Feb 2013.